Age duration and depositional history of the Lower Muschelkalk of Winterswijk

Master thesis final version

Name Student: S.W. Mijnen

1e Supervisor: dr. Bas van de Schootbrugge

2e Supervisor: prof. dr. Jelle Reumer

Date: 11-7-2017

Abstract

If one wishes to fully understand the sedimentation of the Lower Muschelkalk and evolution of the Germanic basin during the Middle Triassic, it crucial to know how long the deposition of the Lower Muschelkalk has taken place. While this has been studied for the center of the Germanic basin, this is not the case for sites located at the edge of the basin. This included the Lower Muschelkalk of Winterswijk, for which there is currently no duration known. In the quarry of Winterswijk the Lower Muschelkalk consists of a 40 meter thick deposit of micritic (marly) limestones, interchanges with several claystones and dolostones. A XRF-scan was executed on a core taken right next to the quarry to trace cyclicity within the geochemical composition of the section. The ratios of cycle-periods in the depth domain were compared with known astronomical periods from the Middle Triassic. This indicates that the thick claystone intervals that are present in the Lower Muschelkalk from Winterswijk represent the 405 kyr eccentricity cycle with a high probability. The whole duration of the deposition would then be ± 1 Myr. Comparisons with German Lower Muschelkalk sections strengthen this hypothesis. From geochemical profiles and calculated sedimentation rates it is proposed that astronomical climate forcing induces changes in lithology by sea level rise and fall.

Contents

1. Introduction

1.1 Goal of the thesis

The Lower Muschelkalk of Winterswijk (LMW) has been extensively studied by geologists, palynologists and paleontologists in the past few decades (Visscher and Commissaris, 1968; Peletier and Kolstee, 1986; Oosterink, 1986; Diedrich, 2001; Herngreen et al., 2005). It is part of the Lower Muschelkalk formation that has been deposited in the Germanic basin of Central Europe during the Middle Triassic (Fig.1) (Peletier and Kolstee, 1986, Oosterink 1986, Hagdorn, 1991, Borkhataria et al, 2006). Lower Muschelkalk sections in Germany have already been studied on the presence of cyclicity to determine their duration, yielding durations of approximately 2 – 3 Myr for the entire Lower Muschelkalk sequence (Götz, 1994, Götz and Feist-Burkhardt, 1999, Götz, 2002, Bachmann and Kozur, 2004). However, these sections were all located in the center of the basin, while the locality of Winterswijk was situated at the edge, close to landmasses. Therefore, climatic and environmental circumstances at Winterswijk may differ from those deeper in the basin, and hence the duration of the LMW deposition may be different from the Lower Muschelkalk sections deeper in the basin. Determining the LMW duration will therefore not only contribute to a better understanding of the duration and evolution of the depositional system on a local scale, but it will also add to the bigger picture of understanding the entire Lower Muschelkalk deposition. Despite the research already done on the LMW, a reliable quantification for the duration of its deposition has not been established yet, which will be the main goal of this thesis.

Another reason why the duration of the LMW is important is the timing of the Permian/Triassic mass extinction recovery phase that started at the onset of the Triassic and was still taking place during the LMW deposition. This is indicated by the biostratigraphy once established by Oosterink (1986); at the bottom, the fossil content is very scarce in both numbers and species, gets more diverse and numerous towards the top. However, it is unknown how long Permian/Triassic mass extinction recovery phase in Central Europe lasted. Therefore, an accurate age model for the LMW will allow a more precise timing and duration for the end of the Permian/Triassic mass extinction recovery phase.

1.2 Approach

In this thesis, cyclostratigraphic analysis is applied to determine the duration of the deposition of the LMW. This method identifies cyclic variations within the lithology and proxy data of the LMW and evaluates if these variations can be linked to durations of astronomically controlled climate fluctuations as described by Milankovitch (1941) and Meyers (2015). Earlier studies already applied cyclostratigraphic to German sections of the Lower Muschelkalk (Götz, 2002; Götz and Török, 2008) and based on the timescale of Gradstein et al. (1995) and Menning (1995) sedimentary cycles of several meters thickness could be tuned to the 100 kyr eccentricity cycle. Even if absolute age control is absent, the bedding hierarchy relationships can be tested for the presence of astronomically induced climate control (Meyers, 2015). This is done by comparing frequency ratios or bundling within lithological data with the known astronomical periodicities of: eccentricity (405 kyr, 100 kyr), obliquity (41 kyr) and precession (21 kyr) (Milankovitch, 1941, Meyers, 2015). By examination of possible fits between periodicities in the depth domain, whether lithological or proxy data, and the astronomical periods, absolute durations may be given to in-depth frequencies. In addition to that, this method also yields feasible sedimentation rates required for the depth-time conversion (Meyers, 2015) and thus an average sedimentation rate for the LMW depositional system.

A problem with lithological data in cyclostratigraphy is that large scale lithological cycles are often well recognizable, but smaller scale cycles may not be as well presented. To tackle this problem, high resolution proxy data is required. Thanks to the development of the XRF-core scanning technique over the last decades, a new method that can analyse geochemical composition with high resolution has become available (Richter et al, 2006). This method has already been successfully used in many paleoclimatic studies (Croudace and Rothwell, 2015) and will also be used in this study on a core drilled right next to the quarry. Applying XRF-core scanning technology will yield an entire new dataset for the LMW set for this section, because this method, or any extensive geochemical analysis for that matter, has never been done before on this section. The expected result is a geochemical data set of about 30 different elements for the entire Upper-Röt (uppermost Buntsandstein) and LMW section of the quarry of Winterswijk with a 1 cm resolution. This dataset may reveal both large and small scale cyclicity within the record that is not visible with the naked eye. Furthermore, the geochemical composition of the lithology also serves as an environmental and climatic fingerprint, which can significantly contribute to the reconstruction of evolution of the LMW depositional environment (Croudace and Rothwell, 2015).

1.3 Geological setting

1.3.1 Winterswijk quarry

The Upper-Röt and LMW are exposed in the quarry next to the Dutch town of Winterswijk. The Röt is a dominantly terrestrial deposit that consists of red claystone that was formed under hot and dry climatic conditions. These claystones are alternated with multiple anhydrite layers that were deposited in hypersaline shallow waters (Oosterink, 1986). The presence of these layers indicates that a marine influence was already present by the time of the Röt deposition. Fossils of any kind are completely absent in the Röt; confirming the fact that the climate and environment must have been uninhabitable for most lifeforms (Peletier and Kolstee, 1986). Ongoing transgression resulted in a facies shift from the dominantly terrestrial environment of the Röt deposition into the shallow marine conditions in which the LMW was deposited. The LMW consists of a ± 35 meter thick layer of limestones and marls interbedded with multiple hard dolostones and red clay layers (Peletier and Kolstee, 1986, Oosterink, 1986). Very abundant and peculiar is the occurrence of Microbially Induced Sedimentary Structures (MISS) within the Muschelkalk deposits (Petelier et Kolstee, 1986, Oosterink, 1986), which are the result of the interaction between microbes and (post) sedimentary processes. From multiple different layers of the LMW pollen, macrofossils and track beds have been sampled and studied (Visscher and Commissaris, 1959, Peletier and Kolstee, 1986, Oosterink, 1986, Diedrich, 2001, Herngreen et al., 2005).

Palynological research done by Visscher and Commissaris (1968) showed that the pollen assemblage of the LMW is similar to Röt-Lower Muschelkalk transitions found in cores in the Eastern Netherlands. Based on these data Visscher and Commissaris (1968) supposed that the age of the Muschelkalk in Winterswijk must be similar to this transition, hence it is considered to be Lower Muschelkalk. However, Visscher and Commissaris (1968) already stated that the accuracy of the LMW pollen data is far from perfect. Herngreen et al. (2005) limits the lower and upper boundaries of the LMW to the Bithynian substage of the Anisian (Middle Triassic) based on pollen found in multiple clay layers of the LMW. Nevertheless, apart from these layers the overall pollen content of the LMW is extremely low (Visscher and Commissaris, 1968, Herngreen et al., 2005).

1.3.2 Germanic basin

The LMW was formed at the western edge of the Germanic basin during the Middle Triassic Epoch (Fig. 1) (Peletier and Kolstee, 1986, Oosterink 1986, Borkhataria 2006). This basin contained large parts of central Europe, including Germany, Poland, parts of North-Eastern France and the Lower Countries. Situated at tropical latitudes, approximately 20° N, it was formed during the Late Permian and has been slowly subsiding throughout the Triassic Period (Hagdorn, 1991). After a period of sea level highstand at the end of the Permian Period regression took place in the Early Triassic and the predominantly terrestrial Buntsandstein Formation was deposited. At the onset of the Middle Triassic the basin was flooded by a shallow tropical sea in which the Lower Muschelkalk Formation was formed (Peletier and Kolstee, 1986, Oosterink, 1986, Hagdorn, 1991). By this time the Germanic basin was almost completely enclosed apart from several connections with the Tethys Ocean in the south and east (Fig.1) (Nawrocki and Szulc, 2000, Borkhataria et al., 2006).

2. Methods

2.1 Core drilling and logging

The studied core, codenamed WIN-15-02, was drilled about 50 meters north of the quarry (coordinates: N 51° 58' 06.7, E 006° 46' 50.4", height above sea-level: 42 m) (Fig. 2). The core was divided in 1 meter long sections and transported to the Royal Netherlands Institute for Sea Research (NIOZ) on Texel.

First, a detailed lithological log was made for the lithified part of the core that spawned from 23.65 meter below surface (mbs) to 76 mbs. The core sections were slightly humidified to visualize lithology, colour, grainsize and sediment structures and sprayed with 10 % diluted hydrochloric acid to determine the degree of effervescence of calcium carbonate. Stratigraphic boundaries within the core section were defined based on changes in lithology, colour, hardness and calcium carbonate effervescence. No fossils were detected nor were any significant changes in sedimentary structures and grainsize.

2.2 XRF Scanning process

After the logging was completed the core sections were posited in plastic tubes that were sectioned in half over the length. A sander was used to smooth the rock surface that would be measured, since the XRF scan requires a flat surface to measure on. The rock surface was cleaned with alcohol and covered with thin, ultralene film to prevent contamination of both the scanner and the sample material during the measurement and to further increase surface smoothness. If necessary, loose and unstable parts of the core were stabilised by supporting them with extruded polystyrene foam.

The XRF scanner that was used is the AVAATECH XRF Core-scanner (Richter et al., 2006). This non-destructive and semi quantitative method uses an Rh (Rhodium) X-Ray to detect relative abundances of elements whose atomic number is equal or between that of Mg and U with a resolution of 1 cm. The scanner emits X-ray radiation that changes the arrangement of electrons within the atoms of the core material, which releases electromagnetic radiation in return. The wavelength of this radiation differs per element, so when the XRF spectrum is plotted, radiation peaks within the spectrum can be attributed to the measured elements based on the wavelength of the radiation represented by these peaks. The amplitude of these peaks reflects the concentration of the measured elements (Richter et al., 2006).

First, LIDAR scans were made for each core section to get high resolution pictures for the entire record. Next, the XRF measurement was performed. To detect as many elements as possible, three runs were executed for the entire lithified interval, each run with a different X-ray tube voltage. This was necessary because each set of elements requires a different X-ray intensity to be optimally measured, with heavier elements requiring more energy. The elements ranging from Mg to Mn were measured at 10 kV, the elements ranging from Fe to Pb at 30 kV and the elements from Sr to U at 50 kV (Richter et al., 2006).
Since not all elements measurable could be (well enough) detected within the core, measurements were only gained for: Mg, Al, Si, P, S, Cl, K, Ca, Ti, V, Cr, Mn, Fe, Co, Ni, Cu, Zn, As, Br, Rb, Sr, Zr, Mo, Pd, Cd and Ba.

2.3 Data correction

For each measured element the XRF data was given in counts/centimeter per centimeter depth interval ranging from 23.65 to 76 mbs, as was the total counts/centimeter for each run. The total amount of counts measured in a run varies per centimeter interval, as well between runs, due to surface roughness, cracks and small gaps within the core. This can cause a decrease in the measured amount of counts while in reality elemental concentrations do not alter. To correct for this problem, all element counts are normalized against the total amount of their respective run. This procedure also allows comparison of elements from different runs. Normalised elements are given as (element count/total counts run).

As uneven and/or cracked surfaces disturb proper measurements and result in very low total counts, not all data points gathered were suitable for further interpretation.
To filter out these low counts, the LIDAR pictures were used to link cracked surfaces within the core material with low total counts in the XRF data in Excel. These points were first filtered out manually, but to remain statistically consistent, it was decided that each data point needs at least a certain amount of counts in all three runs to be valid. These minimum values were established based on the results of the manual filtering: 60.000 counts for the 10 kV, 80.000 counts for the 30 kV, and 8000 counts for the 50 kV.

2.4 Ratios and statistical analysis

Elemental ratios that are supposed to yield significant paleoclimatic and cyclostratigraphic information according to Rothwell and Croudace (2015) were calculated and plotted. Log ratios were used over normal ratios, as log ratios show both large and small variations within a data set whereas linear ratios tend to only show large variations (Hennekam and de Lange, 2012).

Ratios data from 23.65 to 62.15 mbs, as this interval corresponds to the LMW (see results), was imported into PAST (PAleontogical STastics), in which Principal Component Analysis (PCA), Correlation and Time-Series analysis were performed. PCA was performed to constrain geochemical end-members for the LWM. For PCA only the elements that are useful for geochemical proxies according to Croudace and Rothwell (2015) were used, which are: Mg, Al, Si, S, Cl, K, Ca, Ti, Cr, Mn, Fe, Br, Rb, Zr, Pb, Sr and Ba. The data were entered in PAST with elements given as element counts/total counts run on the rows and the values with depth on the columns, since PCA in PAST requires items as rows and variables as columns. PCA was executed with variance-covariance matrix, because all the data points have the same unit (element count/total count run).
The correlation function in PAST was used to identify similar trends, including possible cyclicity, between different elements. This was done only for Al, Fe, Si, K, Ti and Fe, as these are elements that are supposed to display strong cyclic behaviour according to Croudace and Rothwell (2015). Identification of strong (anti-)correlations between these elements served to build the Ca/terrestrial proxy (see results) on which spectral analysis was executed.

2.5 Cyclostratigraphic analysis

The TimeOpt function of the program of ASTROCRHON (Meyers, 2014) was used to identify fits between in-depth cyclic variations observed within the LMW lithology and geochemical data and astronomical target periods. This method possesses multiple important advantages; it can be used on untuned spatial data and on datasets from the entire Phanerozoic (Meyers, 2015). TimeOpt also calculates the sedimentation rate(s) at which the best fit(s) between in-depth and astronomical periodicities is given. Optimal sedimentation rates for the amplitude modulation of precession by eccentricity are calculated as well (Meyers, 2015). However, the main goal of this thesis is to evaluate possible durations of cycles in the depth domain, so sedimentation rates that lead to optimisation of the precession modulation will be disregarded.

The Ca/Terrestrial proxy was transferred into the ASTROCHRON program (Meyers, 2014). First the data was linearly interpolated using the linterp function in ASTROCHRON. TimeOpt requires a given range of feasible sedimentation rates to evaluate for a fit between astronomical target periods and observed periodicities. Based on studies done by Sadler (1999) and Kemp (2012) on average sedimentation rates on Milankovitch times scales in shallow marine carbonate settings, and studies done on Latemar cycles by Preto et al. (2001), minimum and maximum values of 3 to 7 cm/kyr respectively were defined for sedimentation rate. Between these two values, 500 values were investigated for the optimization grid. A logarithmic scale for the grid spacing was used to compensate for the fact that rapid variability often occurs on shorter timescales (Meyers, 2015). TimeOpt evaluates eccentricity and precession parameters in the order of decreasing periods 405.7, 130.7, 123.8, 98.9, and 94.9 ka for eccentricity and 23.6, 22.3, 19.0, 18.9 for precession) decreasing period, starting with the 405 kyr long eccentricity cycle. Note that these durations for precession used by the program are the modern values; the durations for the Middle Triassic are a slightly shorter. However, the 405 kyr cycle has remained stable throughout the Phanerozoic (Laskar et al., 2004, Laskar et al., 2011a, Laskar et al., 2011b, Meyers, 2015) and the changes in the other orbital frequencies remain relatively small. The dataset was automatically detrended by the TimeOpt function.

3. Results

3.1 Lithological log

A lithological description was made of the WIN-15-02 core was directly correlated to the log Oosterink (1986) made inside the quarry. This is necessary for the correlation between the geochemical data of the core and the lithology exposed in the quarry (Fig. 3 ; Fig. 4 ; Fig. 5 contain the description and correlation of the LMW).

The most prominent feature of the section was the difference in colour and lithology between the dominantly red-brown claystones from 76 to 62.15 mbs, an d the white-grey, micritic limestones and marly limestones from 62.15 to 23.63 mbs. By comparison with the quarry lithology described by Oosterink (1986), it was declared that the part from 62.15 to 23.63 mbs corresponds to the LMW, while the part below 62.15 mbs represents the Röt Formation. Sub-millimeter scale, horizontal planar laminations occur throughout almost the entire core section. Limestone and marly limestone parts showed strong reaction with 10 % hydrochloric acid, while the other lithologies did not.

The dominantly red-brown part ranging from 76 to 62.15 mbs starts off with half a meter of fine grained siltstone followed up by claystone up to 63.35 mbs. This claystone layer is finer grained than the underlying siltstone and is alternated with three pink gypsum layers with a thickness ranging from 6 cm for the uppermost gypsum layer to 25 cm for the lower most gypsum layer. The interval from 74.80 to 72 mbs shows a greyer tint in colour than the red-brown deposits both on top and below it. Also, gypsum nodules and concretions can be abundantly found within the silt- and limestone. Above 71.15 mbs up to 63.35 the gypsum nodule density decreases with higher stratigraphic position. From 67.89 to 65.79 mbs there is mudstone layer that shows some small scale flow structures in ominous directions. This layer is greyer in colour than the surrounding layers. A breccia layer, of about 5 cm occurs at 63.35-63.30 mbs and is overlain by a thin 9 cm layer of siltstone that shows some disturbed laminations. From 63.35 to 62.15 mbs there is a dark grey-red dolostone with white and red interchanges and that has high clay content.

From 62.15 mbs the stratigraphic units in de WIN-15-02 are linked to the log once made by Oosterink (1986). It starts with a 215 cm thick dark grey siltstone layer which corresponds to Oosterink bed 1. Following is an 88 centimeter thick dolostone layer up to 59.12 mbs that has a white colour and contains celestine nodules. This dolostone layer is coherent with the

Dolomite I and Oosterink bed 2. A red-brown coloured claystone of 161 cm thick and enriched in nodules follows on top of that, corresponding to Oosterink bed 3. This layer is overlain by a thinner, 19 cm thick claystone layer with a grey colour that is still coherent with Oosterink bed 3. This layer ends at 57.32 mbs. From 57.32 to 53.83 mbs a thick limestone layer occurs that shows bioturbation from 55.78 to 54.57 mbs, with increasing intensity toward the top. This thick limestone layer corresponds to Oosterink beds 4-10 and is overlain by a red-brown claystone layer of 34 cm thickness, corresponding to Oosterink bed 11.

The section from 53.83 to 52.04 mbs consists of marly limestone with a darker grey colour interval from 53.37 to 53.00 mbs, corresponding to Oosterink bed 12. This layer is overlain by the Dolomite II layer that is 62 centimeters thick, which is coherent with Oosterink bed 13. On top of that follows a deposit consisting of marly limestone of 142 centimeters thick. These deposits are hard to correlate with the Oosterink stratigraphy but this interval is at least coherent with Oosterink beds 14-19. Next are two marly limestone layers of 132 and 125 mbs thick respectively, with a claystone layer situated in between them ranging from 46.68 to 48.35 mbs in between them. This entire interval corresponds to Oosterink bed 20 and ends at 47.10 mbs. The uppermost marly layer also contains white spots and shaly structures. This is followed up by a thin grey clay layer, corresponding to Oosterink bed 21 of 17 cm thick. Super posited on that are two white grey coloured dolostone layers of 46.4 and 45.25 centimeter thick respectively and are coherent with the Dolomite III and IV and Oosterink beds 22 and 24. In between them is a dark mudstone interval, with strange shale like structures, corresponding to Oosterink bed 23. On top of these dolostones another dark, calcareous mudstone layer is situated that shows solution holes and ranges from 45.25 to 44.4 mbs. It is unclear whether this interval corresponds to either Oosterink bed 25 or 28 because a limestone interval like Oosterink bed 26 and a galenite bed corresponding to Oosterink bed 27 could not be found within the core. Their determination would require further research.

The next interval is a marly limestone with a light gray colour of 110 centimeter that ends at a stratigraphic position of 43.30 mbs, corresponding to Oosterink beds 30-32. It is overlain by a 530 centimeter thick deposit of hard limestone with a white to light grey colour that corresponds to Oosterink beds 33 and 34. This thick interval ends at 38 mbs. A galenite bed corresponding to Oosterink bed 35 has not been found.

From 38 mbs to 37.22 mbs there is a marly limestone layer that has a very light white-grey colour, correspond to Oosterink bed 36). An interval of 222 centimeter of light grey limestone is situated on top of that. This limestone layer is overlain by two marly limestone layers; first a white layer of 80 centimeter thick and second a grey layer of 35 centimeter thick. From 33.85 to 33 mbs there is a dark claystone layer. This layer is overlain by another light grey limestone layer of 230 centimeter thick which ends at 30.70 mbs. The entire interval from 37.22 to 30.70 mbs corresponds to the Oosterink intervals 37-39, although the dark grey clay layer has never been described by Oosterink (1986).

From 30.70 to 30 mbs there is a dark grey dolomitic interval that is coherent with Dolomite V as described by Oosterink (1986). This is where the correlation with Oosterink (1986) ceases. Following up is a light grey, massive limestone of 185 cm and a brittle claystone of 85 centimeters thick. The top of the core, ranging from 27.3 to 23.65 mbs, consists of grey, marly limestone and there is sharp unconformity with the overlaying and unlithified Rhaetian clays.

3.2 Geochemical ratios

The proxies shown in (Fig. 4 ; Fig. 5) were chosen as they were supposed to cover as much paleoenvironmental information as possible. Ca/Fe, Ca/Ti and Ca/Al were all chosen as indicators of marine vs terrestrial input in the system. Ca origins from in-situ carbonate precipitation (Nichols, 2009) while Fe, Ti and Al represent terrestrial input and therefore they can also reflect continental weathering (Croudace and Rothwell, 2015). The Ca ratios show large negative shifts at the claystone intervals (Fig. 4 ; Fig. 5). This fits with the lithological observations, as claystones are typically enriched in terrestrial elements and diluted in calcium. The Si/Al proxy was shown to reflect grainsize variations (Fig. 4). It becomes more negative in the claystone intervals that typically have a higher Al content. Besides that, Si/Al remains constant for the rest of the core as there are no significant changes in grainsize present. K/Ti reflects continental weathering regimes (Fig. 4). Higher abundances of Ti, a coarse compound, could reflect enhanced continental weathering. K/Ti shows negative shifts around the claystone intervals, which may indeed be intervals of enhanced continental weathering (Croudace and Rothwell, 2015). Ca/Mg was plotted for dolostone identification, as dolostones are enriched in Mg (Fig. 5). However, Mg is also high for claystone intervals, therefore Mg/Al was plotted, which shows high values for the dolostone intervals. Fe/K was plotted to reflect hinterland humidity (Fig. 5) (Croudace and Rothwell, 2015), but it does not show any significant changes throughout the core.

3.3 Ca/Terrestrial proxy

Four different end-members for the LMW depositional system can be concluded (Table 1 ; Fig. 6). Ca/total is the most distinctive end-member in this case, being responsible for most of the variation explained by PC1 and therefore in the entire LMW system. Sr/total is the second most distinctive element and causes most of the variation related to PC2. The third end-member of the system is Fe/total which has slightly higher values for PC1 and PC2 two than the other elements, except for Ca/total. The remaining elements are grouped together as their contribution to variations in the system is very small compared to Ca/total, Sr/total and Fe/total (Fig. 6).

For an accurate cyclostratigraphic interpretation of the dataset a proxy that shows possible cyclicity as good as possible needs to be established. Al, Si, K, Ca, Ti and Fe are all elements that have shown to strongly display cyclicity in past paleoclimate studies (Croudace and Rothwell, 2015).
Ca/total is a different endmember of the system that the other elements (Fig. 6). It can also be seen that there is a highly negative correlation between Ca/total and any one of Al/total, Si/total, K/total, Ti/total and Fe/total (Table 2). Therefore, it is feasible that cyclicity is best expressed in a ratio of Ca/total over these elements.

Because of the overwhelming abundance of Ca/total within the WIN-15-02 core, ratios as Ca/element'X' tend be overshadowed by fluctuations within Ca/total. To tackle this problem, a sum was taken over Al/total, Si/total, K/total, Ti/total and Fe/total. These elements show similar in-depth profile and highly positive correlations with each other (Fig. 4 ; Fig. 5 ; Table 2). By doing this, small perturbations in the abundance of these elements can now better be seen when plotting them in a ratio over Ca/total. This method assumes that all five terrestrial elements have similar in-depth perturbations, which, again based on their high correlation (0.90+) and similar in-depth geochemical profiles, is a safe assumption to make (Table 2). A log ratio was used because as explained in the methods, log ratios display both large and short scale variations.

3.4 Analysis in the depth domain

A spectral analysis of the Ca/Terrestrial proxy was made to show the dominant periodicities in the depth domain (Fig. 7 ; Fig. 8). Major peaks occur at frequencies of $8.33*10^{-4}$, $1.62*10^{-3}$, $2.04*10^{-3}$, $2.46*10^{-3}$ and $2.87*10^{-3}$, all in units of 1/cm, which correspond to periodicities of

12.0, 6.2, 4.9, 4.1 and, 3.5 meter. Minor peaks occur at $3.34*10^{-3}$, $3.68*10^{-3}$, $5,39*10^{-3}$, $6.14*10^{-3}$ and $6.51*10^{-3}$, again in units of 1/cm, which yield periodicities of 3.0, 2.7, 2.2, 1.8, 1.7, 1.5 and 1.1 meter. These peaks could later be coupled to the ASTROCHRON spectral analysis profiles in the time domain.

3.5 Cyclostratigraphic results

R^2 power evaluates the quality of the fit between in-depth cycles and the target astronomical periods for each given sedimentation rate (Fig. 9). R^2 power has a peak value at a sedimentation rate of 3.6 cm/kyr. However, R^2 envelope, which identifies fits for eccentricity modulated amplitude within the precession band, has peak values at much higher sedimentation rates, resulting in a peak value for sedimentation rate of 7 cm/kyr derived for the optimal fit (Fig. 9). This sedimentation rate does not to yield a good fit between astronomical periods for eccentricity and the highest spectral power peaks. The precession signal seems to be weakly present as indicated by several small peaks within the precession band, but by far not as strong spectral components at lower frequencies (Fig. 9). Therefore, the accuracy of the sedimentation rate fits indicated by the R^2 envelope seems to be rather unreliable and thus insignificant for the fit between eccentricity periods with high spectral power peaks. The values for sedimentation rate were limited to the area around 3.6 cm/kyr, where the best fit between peak spectral power and astronomical periods is to be expected.

To investigate fits around the R^2 power peak value, the range of sedimentation rates was shortened to 3 to 4 cm/kyr. By this modification, high peak values in the R^2 envelope could now be ruled out, allowing an evaluation for fits between the spectral power and target astronomical periods at R^2 spectral power peak value.

The peak in R^2 power is again present at a sedimentation rate of 3.6 cm/kyr, while the peak of R^2 envelope is situated at the same value, yielding an optimal fit at a sedimentation rate of 3.6 cm/kyr on which the power spectrum is based (Fig. 10). Now, a perfect fit is present between the period of 405 kyr and the highest spectral power present in the proxy-record. The short eccentricity periods fall in the range of the fourth and fifth spectral peaks (from lower to higher frequency) in the proxy record (Fig. 10). No peaks are present at the precession band for this range of sedimentation rates.

A third run was executed to evaluate the case that the longest astronomical frequency present within the record is a short eccentricity period instead of the 405 kyr cycle. The maximum sedimentation rate for investigation was therefore increased to 12 cm/kyr, as this is the highest feasible sedimentation rate on Milankovitch time scales according to Sadler (1999) and Kemp (2012).

The peak in R^2 power is now present at an average sedimentation rate of 4.7 cm/kyr, although the entire interval from 4 to 8 cm/kyr yields high values for R^2 power (Fig. 11). R^2 envelope reaches its highest value at 12 cm/kyr, yielding an optimal fit at a sedimentation rate of 11.8 cm/ka. For this sedimentation rate the strongest spectral component fits perfectly with the short-term eccentricity periods, while the precession periods fit with several small peaks within the precession band (Fig. 11). However, no astronomical target period of neither eccentricity nor precession is coherent with the second, third, fourth and fifth spectral peaks (from lower to higher frequency) (Fig. 11).

4. Discussion

4.1 Duration of the LMW deposition

TimeOpt suggests that the best fit between astronomical target periods and in-depth cyclicity is given at an average sedimentation rate of 3.6 cm/kyr (Table 3 ; Fig. 10; Fig.14). For this value, the long eccentricity cycle corresponds closely to the 12 meter claystone intervals (Fig. 12). Subsequently, the short eccentricity cycle would have an in-depth period of 3.4 to 4.5 meter which agrees with the 3.5 – 4.1 meter cycle found within the Ca/Terrestrial proxy. Precession and obliquity cycles, that would have periods of 40 kyr and 24 - 19 kyr for the Middle Triassic respectively (Meyers, 2015) are not distinguishable (Table 3; Fig, 11). For the LMW deposition with an average sedimentation rate of 3.6 cm/kyr a duration of roughly 1 Myr is given.

When the 12 meter claystones are linked to short eccentricity (leaving out the long eccentricity), TimeOpt suggests that the best fit is given at an average 12 cm/kyr (Fig. 10). In this case, the 12 meter cycle should reflect the shorter eccentricity period (94.9 and 98.9 kyr) to still have a good fit, as the sedimentation rate would be too high to correspond to other short eccentricity periods. Precession would be expressed with an interval of 1.9 to 3 meter, which is not present within the in-depth record and too short to correspond well with the 3.5 – 4.1 meter cycle. Furthermore, the spectral power within the precession domain is weak (Fig. 10). The long eccentricity cycle should occur over an interval of 52.5 meter, but no such expression is detected within the lithology or the proxy data. Its period could either be too long, as it exceeds the length of the record, or its influence too weak to be registered. It is unlikely that the latter would the case, as past studies suggest that the 405 kyr cycle is the most stable and well recognisable astronomical period in ancient sediment records (Olsen and Kent 1999, Laskar et al., 2004, Ikeda, 2010, Laskar et al., 2011a, Laskar et al., 2011b, Ikeda & Tada, 2012). For an average sedimentation rate of 13 cm/kyr the entire LMW deposition would have taken about 256 kyr. According to Sadler (1999) and Kemp (2012) this value for sedimentation rate is high for the considered timescale. Based on the poor fit between in-depth cyclicity and astronomical target periods, no identifiable long eccentricity cycle within the depth record and high sedimentation rates for the timescale considered, it is unlikely that the 12 meter cycle would correspond to a short eccentricity period.

Pietersen (2010) has also studied cyclicity in the quarry of Winterswijk based on lithological observations. Pietersen (2010) defined cycles of 5 to 6 meter thickness, consisting of marls with two resistant beds at the top with a fine grained layer in between them. For the entire LMW 7 to 9 of the cycles were supposed, which were linked to the 405 kyr cycle. This would lead to a total duration for the LMW deposition of 3 to 4 Myr. Compared to the results found in this thesis, this duration seems too long. No 5 to 6 meter cycles were found in the lithology nor geochemistry and it is not clear on what Pietersen (2010) based the link between the long eccentricity and these 5 to 6 meter cycles. Therefore, the by Pietersen (2010) proposed duration of 3 to 4 Myr for the LMW deposition seems to be too unreliable.

4.2 Correlation within the Germanic basin

Studies by Götz (2002) on sections in Germany defined transgressive-regressive cycles of several meters thick as the basic units for the Lower Muschelkalk. These units can be very well identified and correlated throughout the entire Germanic basin (Götz, 2002). Therefore Götz (2002) suggested that an auto cyclic cause for their formation is unlikely. At least 20 of these so called Kleinzyklen have been identified for the entire Lower Muschelkalk formation within the Germanic basin (Götz 1994, Götz and Feist-Burkhardt 1999). Based upon research of Gradstein et al. (1995) and Menning (1995), Götz (2002) and Bachmann and Kozur (2004) assumed a duration of 2 – 3 Myr for the entire Lower Muschelkalk, with the Kleinzyklen reflecting the short-eccentricity cycle. When comparing these Kleinzyklen to the LMW formation, they are similar to the 3.5 - 4.1 meter cycle in both thickness as well lithology, as both units consists of micritic limestones (Fig. 12). Because of the similar lithology it can be assumed that sedimentation rates for both units are of comparable magnitude as well. This strengthens the hypothesis that the 3.5 – 4.1 meter cycle in the LMW corresponds to the short eccentricity cycle like the Kleinzyklen do.

4.3 Evolution of the LMW depositional system

Variations in sedimentation within a shallow marine carbonate system are determined by variations in sediment supply and the available accommodation space. Sediment supply comes from both in-situ formed carbonate and terrestrial weathering, which are indirectly controlled by variations in climate (Croudace and Rothwell, 2015). The available accommodation space is controlled by changes in relative sea level caused by both climatic and tectonic processes (Götz 2002, Kemp 2012). Overall, long-term changes in accommodation space are caused by tectonic rise and subsidence of the seafloor. Shifts in lithology, on the other hand, are caused by astronomically induced climate changes via variations in eustatic sea level or sediment supply (Strasser et al., 2000).

Shallow marine carbonate systems only occur on carbonate shelfs during periods of sea level highstand during which the shelfs are flooded and carbonate can be produced (Nichols, 2009). Therefore, the (marly) limestones of the LMW will reflect transgressive and highstand systems tracts. Götz (2002) defined that the Kleinzyklen found in German Lower Muschelkalk sections consist of a highstand systems tract reflected by meters thick micritic limestones and a transgressive systems tract represented by a bioclastic chalk bank over several decimeters thickness. These bioclastic chalk beds were not defined within the WIN 15-02 core. Lowstand and Regressive Systems Tracts are absent in the Kleinzyklen (Götz, 2002), as during phases of sea level lowstand no deposition occurs on the shelf areas.

4.4 Astronomical-lithological phase relations

An idea for the phase relation between astronomical parameters and the lithology is by climatic induced sea level rise and fall. During sea level rise, micritic limestones are deposited on carbonate shelfs (transgressive and highstand systems tract). Excess of sediment supply over sea level rise during highstand regression would result in a seaward movement of the coastline, which will cause the sediment geochemistry to get a more proximal character. This is reflected by a higher relative abundance of terrestrial elements. During sea level fall, part of the transgressive and highstand deposits would be eroded away and deposition would have taken place in the deeper parts of the Germanic basin, leading to a phase of little to no deposition on the shelf areas. When the sea level rises again, the shelf is flooded and the next sequence of micritic limestones is deposited again. This would create a hiatus between two consecutive limestone sequences containing the regressive, lowstand and part of the highstand systems tract. These hiatuses should be present at the 3.5 – 4.1 peaks and therefore sea level rise and fall should be related to the short eccentricity cycle.

As the large claystone intervals of the 12 meter cycle do not show any reactivity with hydrochloric acid and are so starved in calcium carbonate. Therefore, they are supposed to not have formed on the shallow carbonate shelf, but instead during prolonged periods of emergence of the shelf. This could only have occurred after large sea level drops, which may have formed large hiatuses at the onset of the claystone intervals. The sharp transition in lithology and sediment geochemistry supports the presence of hiatuses at these positions. After emergence the shelf was drowned again due to sea level rise, causing the deposition of new transgressive and highstand limestones on top of the claystone intervals. This cycle of large sea level rise and drops, including emergence of the shelf, would then have been controlled by the long eccentricity cycle and thus is reflected by the claystone intervals every 12 meter.

Another possibility is that astronomical cyclicity controls the amount of terrigenous sediment supply in the LMW system and that claystone intervals are the result of enhanced continental weathering. Winterswijk was located at tropical latitudes during Middle Triassic times where was supposedly a monsoonal system present like in the present (Gradstein et al, 2012). A stronger monsoon causes more terrestrial weathering, enhancing terrestrial element input in the system. These phases of intensified monsoons would be controlled by the precession cycle, which in turn is modulated by the long and short term eccentricity cycles. Hence the intensified monsoon would reflect short and long eccentricity cycles.

A possible explanation of the relation between astronomical influences and sea level variations could be thermal expansion and compaction of seawater. Although this effect may only cause sea level to rise and fall a few meters, such a difference can be quite significant for shallow carbonate platforms. Organisms producing the calcium carbonate often require specific water depth to do so and when the depth is too high or too low, production will cease (Kemp, 2012). Sea level changes induced by large ice sheet growth and melt like during the Quaternary seem unlikely, as they are no known large storages of ice present in the greenhouse Middle Triassic, nor any other alternatives for large scale continental water storage (Gradstein et al., 2012). Enhanced terrestrial input due to intensified weathering has a relatively low influence on in-situ carbonate production, especially compared to the effect of sea level changes. Claystone intervals caused by monsoonal systems are still likely to contain calcium carbonate, which claystones in the LMW do not. Therefore, it is unlikely that the claystone intervals are the result of monsoonal influences.
If the short and long eccentricity cycles control sea level fluctuations in the LMW system, this would have led to a carbonate sequence stratigraphy in which sea level highstand is reflected by limestone deposits, while phases of sea level lowstand are represented by hiatuses and thick claystone intervals for the 405 kyr cycle. In this case, astronomical forcing not only controls phases of sedimentation, but also phases of erosion and no deposition (Sadler, 1999, Kemp, 2012). This astronomically induced formation of hiatuses causes the average sedimentation rate of a section to decrease on Milankovitch timescales. However,

astronomically forced hiatuses occur with a regular period and therefore the astronomical signal remains recognisable within lithology and geochemistry (Kemp 2012). Enhanced monsoonal forcing, on the other hand, does not introduce hiatuses in the LMW systems like a fluctuating sea level would do, so it does not bring hiatuses in the system like carbonate sequence stratigraphy does. These Milankovitch enforced hiatuses in the system are required, however, to get a fit between sedimentation rate and considered timespans on Milankovitch timescales and beyond (Sadler, 1999, Kemp, 2012). Also, if the monsoonal system in the Triassic functioned similar as the current day system, a strong precession component is expected to be present, but it is not well expressed in the LMW. Based on these and aforementioned arguments, sea level fluctuations seem to be a more likely cause for the phase relation between astronomical climate forcing and lithology than a monsoonal influence would be.

Several vertebrate track beds and bone beds have been identified by Diedrich (2001) in the LMW. These beds represent phases when the sea level was shallow enough, including tidal flat conditions, that animals were able to cross over by foot. The occurrence of track and bone beds at certain stratigraphic position indicates that a fluctuating sea level was indeed present during the LMW deposition. Further research is required to investigate if these beds coincide with peaks in terrestrial element abundance, in which case vertebrate migration in the Middle Triassic may be linked to astronomical climate forcing.

4.5 Uncertainties in the quarry

The in-depth cycles in the LMW seem to have constant periods for the interval from 31 to 62.15 mbs. However, in the part of the LMW section above the 31 mbs the cycles are much harder to define. There is a negative peak present at 27.5 mbs of which the amplitude matches the amplitudes of neither the 12 nor the 3.5 – 4.1 meter intervals. Also, its distance of ± 6 meter to the 33 mbs peak does not match any of the two in-depth eccentricity periods and is not recorded elsewhere within the LMW record (Fig. 12).

A possible explanation for the period of this peak could be a change in sedimentation rate. Therefore, the peak could correspond to a long eccentricity cycle by decreasing the sedimentation rate above the 31 mbs, causing the long eccentricity peak to be weaker expressed and have a shorter in-depth period. On the other hand, a higher sedimentation rate at this interval could cause a short eccentricity period to be stronger expressed and also have a longer in-depth period. A third possibility is that there is a strong hiatus present above which the in-depth cyclicity behaves differently from the part below the hiatus. Apart from erosion and non-deposition, possible faults and shear surfaces that occur in the quarry (Oosterink, 1986, Peletier and Kolstee, 1986) could lead to hiatus formation as well. Currently it remains unclear what the main cause is for the change in cyclicity regime.

5. Conclusions

The most likely scenario for an age model for the LMW is a fit between the 12 meter claystone intervals and the 405 kyr eccentricity cycle, according to multiple comparisons between different fits derived from ASTROCRON and given sedimentation rates for shallow carbonate systems. This scenario is also consistent with age models given for German Lower Muschelkalk sections. The total duration for the LMW deposition comes down to about 1 Myr with an average sedimentation rate of ± 3.6 cm/kyr, although there is a lot of uncertainty involving the part of section above the 31 mbs. The explanation given here for the influence of astronomical parameters on the LMW system is that they control phases of sea level rise and fall. With this, phases of carbonate deposition and erosion can be distinguished, and hiatuses are supposed created at Milankovitch timescales.

References

Bachmann, G. H., and H. W. Kozur. "The Germanic Triassic: correlations with the international scale, numerical ages and Milankovitch cyclicity: Hallesches Jahrbuch Geowissenschaften." (2004): 17-62.

Borkhataria, R., T. Aigner, and K.J.C.P Pipping. "An unusual, muddy, epeiric carbonate reservoir: the Lower Muschelkalk (Middle Triassic) of the Netherlands." *AAPG bulletin* 90.1 (2006): 61-89.

Croudace, Ian W., and R. Guy Rothwell, eds. *Micro-XRF Studies of Sediment Cores: Applications of a non-destructive tool for the environmental sciences*. Vol. 17. Springer, 2015.

Diedrich, C. "Vertebrate track bed stratigraphy of the Röt and basal Lower Muschelkalk (Anisian) of Winterswijk (East Netherlands)." *Nordic Journal of Geosciences* 80.02 (2001): 31-39.

Götz, A.E. "Feinstratigraphie und Zyklengliederung im Unteren Muschelkalk (Raum Creuzburg–Westthüringen)." *Beitr Geol Thüringen NF* 1 (1994): 3-12.

Götz, A.E., and S. Feist-Burkhardt. "Sequenzstratigraphische Interpretation der Kleinzyklen im Unteren Muschelkalk (Mitteltrias, Germanisches Becken)." *Zentralblatt der Geologie und Paläontologie, Tail. I* 1997.7-9 (1999): 1205-1219.

Götz, A.E. "Hochauflösende Stratigraphie im Unteren Muschelkalk (Mitteltrias, Anis) des Germanischen Beckens." *Schriftenr. Deutsch. Geol. Ges* 15 (2002): 101-107.

Götz, A.E., and A. Török. "Correlation of Tethyan and Peri-Tethyan long-term and high-frequency eustatic signals (Anisian, Middle Triassic)." *Geologica Carpathica* 59.4 (2008): 307-317.

Gradstein, F.M., Agterberg, F.P., Ogg, J.G., van Veen, P., Thierry, J. and Z. Huang "A Triassic, Jurassic and Cretaceous time scale." (1995).

Gradstein, F.W., Ogg, J.G. Schmitz, M.D and G.M. Ogg: *The geologic time scale 2012*. Elsevier (2012)

Hagdorn, H.: Muschelkalk: a field guide *international Muschelkalk Symposium from 12 to 20 August 1991 in Schöntal, Jagst*. Goldschneck-Verlag Weidert, (1991).

Hennekam, R., and G. de Lange. "X-ray fluorescence core scanning of wet marine sediments: methods to improve quality and reproducibility of high-resolution paleoenvironmental records." *Limnol. Oceanogr. Methods* 10.12 (2012): 991-1003.

Herngreen, G. F. W., van Konijnenburg-van Cittert, J. H. A. and H. W. Oosterink. "New geological data (Middle Triassic, Rhaetian-Liassic and Oligocene) of the Winterswijk quarry, the eastern Netherlands." *Netherlands Journal of Geosciences* 84.04 (2005): 409-413.

Ikeda, M., Tada, R., and H. Sakuma. "Astronomical cycle origin of bedded chert: a middle Triassic bedded chert sequence, Inuyama, Japan." *Earth and Planetary Science Letters* 297.3 (2010): 369-378.

Ikeda, M., and R. Tada."Long period astronomical cycles from the Triassic to Jurassic bedded chert sequence (Inuyama, Japan); Geologic evidences for the chaotic behavior of solar planets." *Earth*, *Planets and Space* 65.4 (2013): 351.

Kemp, David B. "Stochastic and deterministic controls on stratigraphic completeness and fidelity." *International Journal of Earth Sciences* (2012): 1-14.

Laskar, J., Robutel, P., Joutel, F. Gastineau, M., Correia, A.C.M. and B. Levrard. "A long-term numerical solution for the insolation quantities of the Earth." *Astronomy & Astrophysics* 428.1 (2004): 261-285.

Laskar, J., Fienga, A., Gastineau, M. and H. Manche. "La2010: a new orbital solution for the long-term motion of the Earth." *Astronomy & Astrophysics* 532 (2011): A89.

Laskar, J., Fienga, A., Gastineau, M., Delisle, J.-B. and A. Farres "Strong chaos induced by close encounters with Ceres and Vesta." *Astronomy & Astrophysics* 532 (2011): L4.

Menning, Manfred. "A numerical time scale for the Permian and Triassic periods: an integrated time analysis." *The Permian of Northern Pangea*. Springer Berlin Heidelberg, (1995). 77-97.

Meyers, S. R. "Astrochron: An R package for astrochronology." *Available at c ran. rproject. org/web/packages/astrochron/index. html* (2014).

Meyers, S.R. "The evaluation of eccentricity-related amplitude modulation and bundling in paleoclimate data: An inverse approach for astrochronologic testing and time scale optimization." *Paleoceanography* 30.12 (2015): 1625-1640.

Milanković, M. *Kanon der Erdbestrahlung und seine Anwendung auf das Eiszeitenproblem*. na, 1941.

Nawrocki, J. and J. Szulc. "The Middle Triassic magnetostratigraphy from the Peri-Tethys basin in Poland." *Earth and Planetary Science Letters* 182.1 (2000): 77-92.

Olsen, P. E., and D. V. Kent. "Long-period Milankovitch cycles from the Late Triassic and Early Jurassic of eastern North America and their implications for the calibration of the Early Mesozoic time–scale and the long–term behaviour of the planets." *Philosophical Transactions of the Royal Society of London A: Mathematical, Physical and Engineering Sciences* 357.1757 (1999): 1761-1786.

Oosterink, H. W. "Winterswijk, geologie deel II. De Trias-periode (geologie, mineralogie en fossilien)." *Wetenschappelijke Mededelingen Koninklijke Nederlandse Natuurhistorische Vereniging* 178 (1986): 1-120.

Peletier, W and H.G. Kolstee: Winterswijk, geologie deel I.. *Wetenschappelijke Mededelingen Koninklijke Nederlandse Natuurhistorische Vereniging* (1986)

Pietersen, J. “Stratigraphy and sedimentology of the Middle Triassic Muschelkalk facies in the Winterswijk quarry, East Netherlands” Bachelor Thesis, Vrij Universiteit Amsterdam (2010).

Preto, N., Hinnov, L.A., Hardie, L.A. and V. de Zache: "Middle Triassic orbital signature recorded in the shallow-marine Latemar carbonate buildup (Dolomites, Italy)." *Geology* 29.12 (2001): 1123-1126.

Sadler, P. M. "The influence of hiatuses on sediment accumulation rates." *GeoResearch Forum*. Vol. 5. No. 1. 1999.

Strasser, A, Hillgärtner, H., Hug, W. and B. Pittet: "Third-order depositional sequences reflecting Milankovitch cyclicity." *Terra Nova* 12.6 (2000): 303-311.

Richter, T.O., van der Gaast, S., Koster, B., Vaars, A., Gieles, R., de Stigter, H.C. de Haas, H. and T.C.E. van Weering: "The Avaatech XRF Core Scanner: technical description and applications to NE Atlantic sediments." *Geological Society, London, Special Publications* 267.1 (2006): 39-50.

Visscher, H., and A. L. T. M. Commissaris. "Middle Triassic pollen and spores from the Lower Muschelkalk of Winterswijk (the Netherlands)." Mededelingen van het Botanisch Museum en Herbarium van de Rijksuniversiteit te Utrecht 307.1 (1968): 161-176.

Appendix:

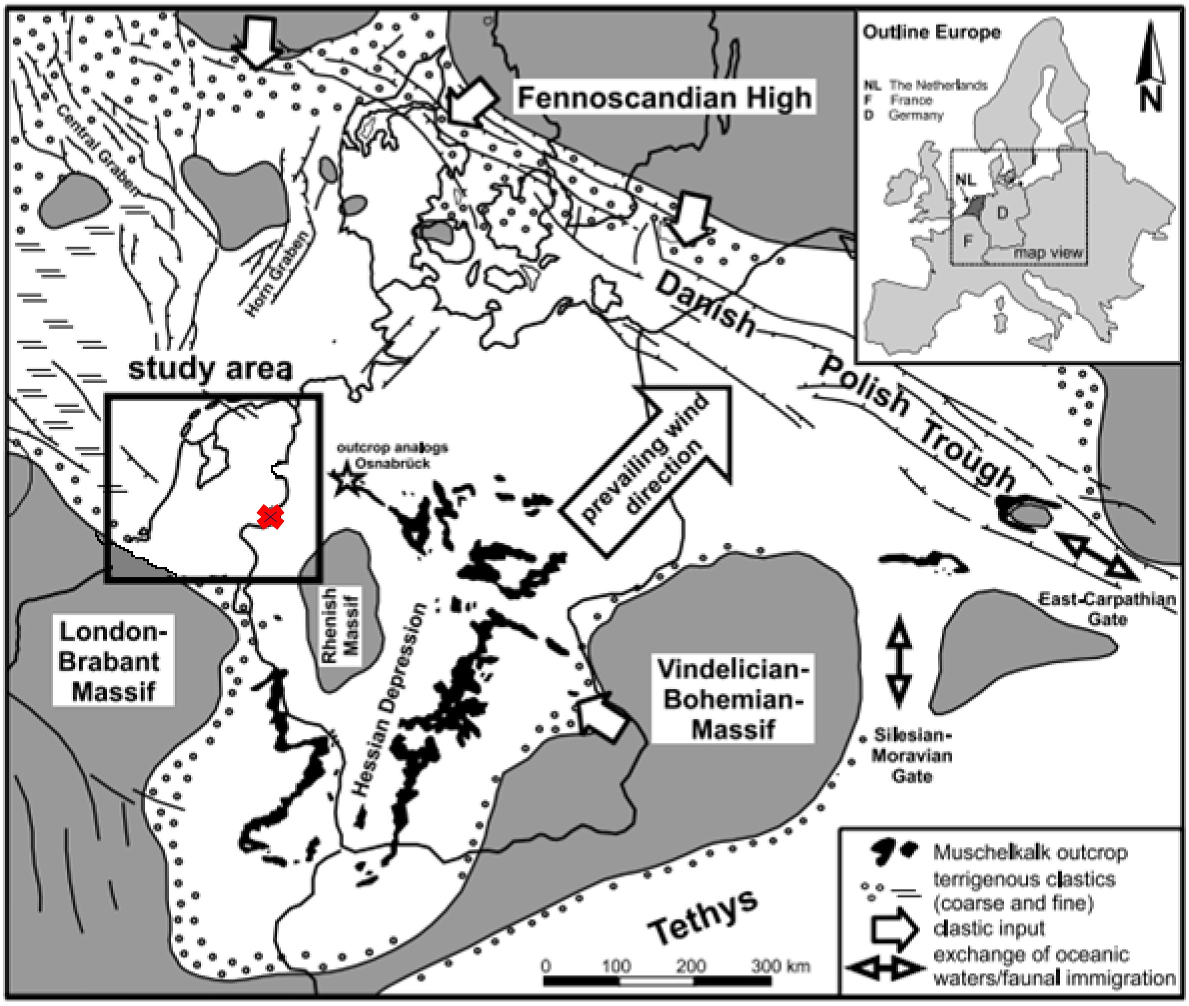

Fig. 1: Paleogeographical overview of the Germanic basin during the timing of the Lower Muschelkalk deposition modified after Borkhataria et al. (2006). Shown are the most important land masses, seaways, wind direction and current borders of the Netherlands and Germany. The red cross indicates the location of Winterswijk, at the western margin of the basin.

Fig. 2: Location of the WIN15-02 as indicated by the red marker. The quarry is located in the south-east corner

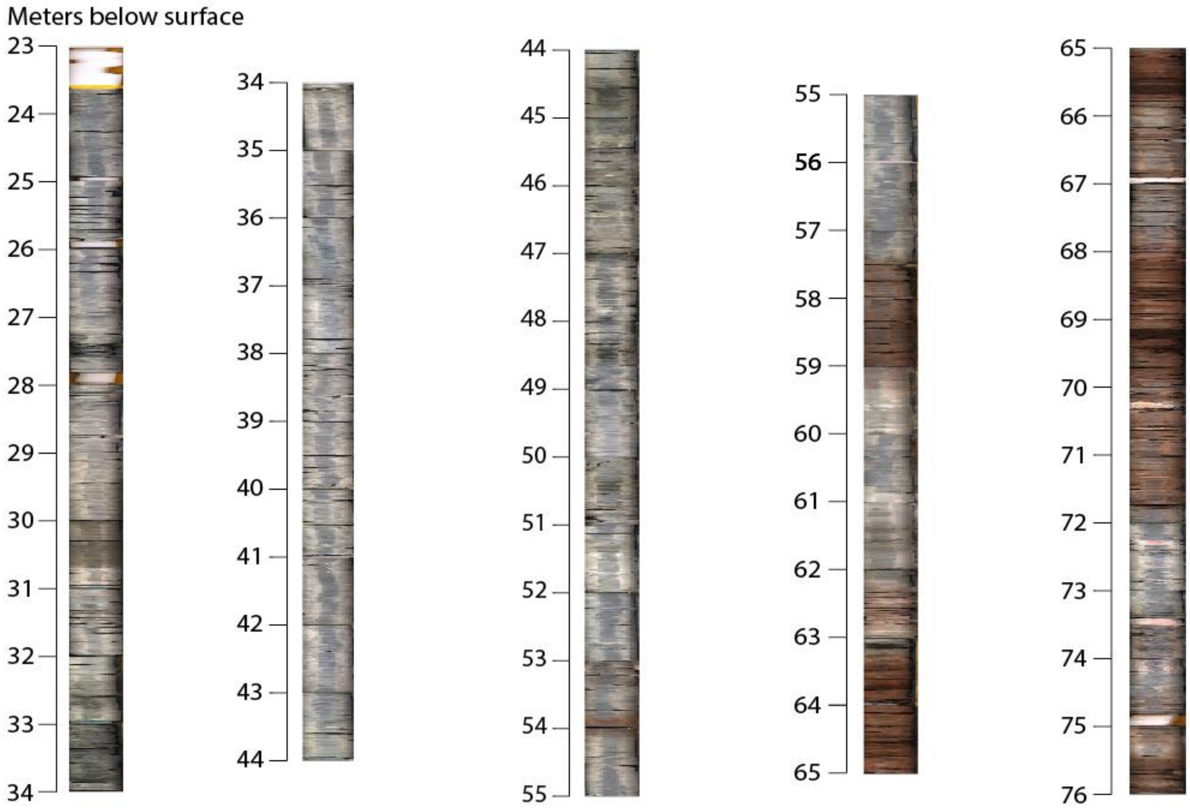

Fig. 3 Photo log of the compiled LIDAR pictures of the WIN-15-02 core, showing changes within lithology and colour down core. The bar indicates meters below surface. Foam pieces were used to support the core material within the liner where needed.

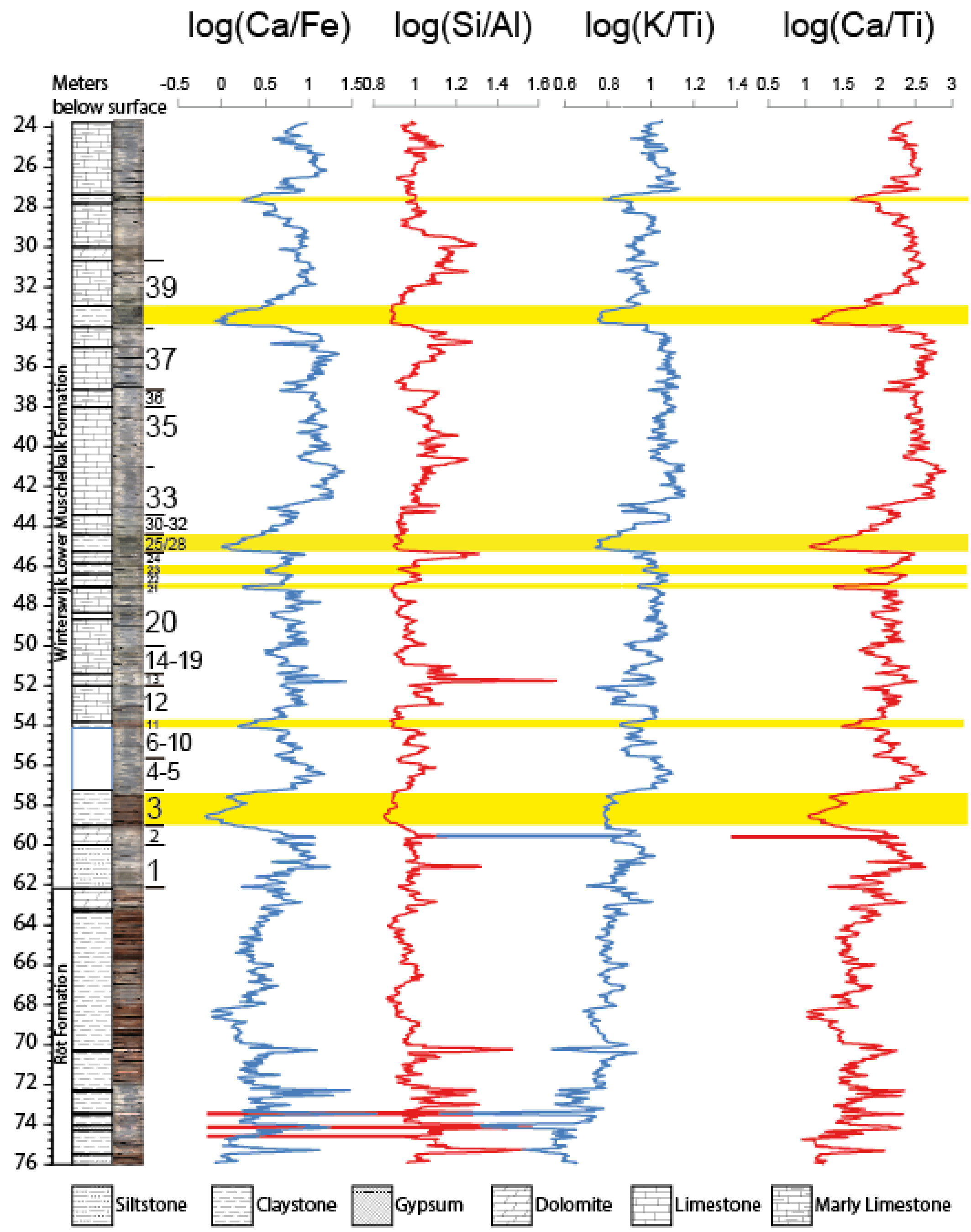

Fig. 4: Log of the LMW with several geochemical ratios. Left: the lithological log and photo log that show the dominant lithologies and colours with depth surace and the formations which they belong to. The numbers show the correlation between the WIN-15-02 core and the Oosterink units in the quarry (Oosterink, 1986). Therefore, it is possible to correlate the core to the quarry directly. Depth was given in meters below surface.

For geochemical analysis only the LMW part is considered. Ca/Fe and Ca/Ti are proxies that show the marine (biogenic) vs terrestrial (lithogenic) input. Negative shifts, which indicate intervals of terrestrial over marine input, are coherent with claystone intervals within the lithology as indicated by the yellow bars. The Si/Al proxy indicates grainsize, with Si representing larger clasts and Al the lower smaller clasts respectively. Save for some small negative shifts in the claystone intervals the grainsize does not change significantly throughout the core. K/Ti can be used as a measure for continental weathering, whereas negative shifts indicate enhanced weathering. These are present for the claystone intervals, but the proxy shows constant values for the rest of the core.

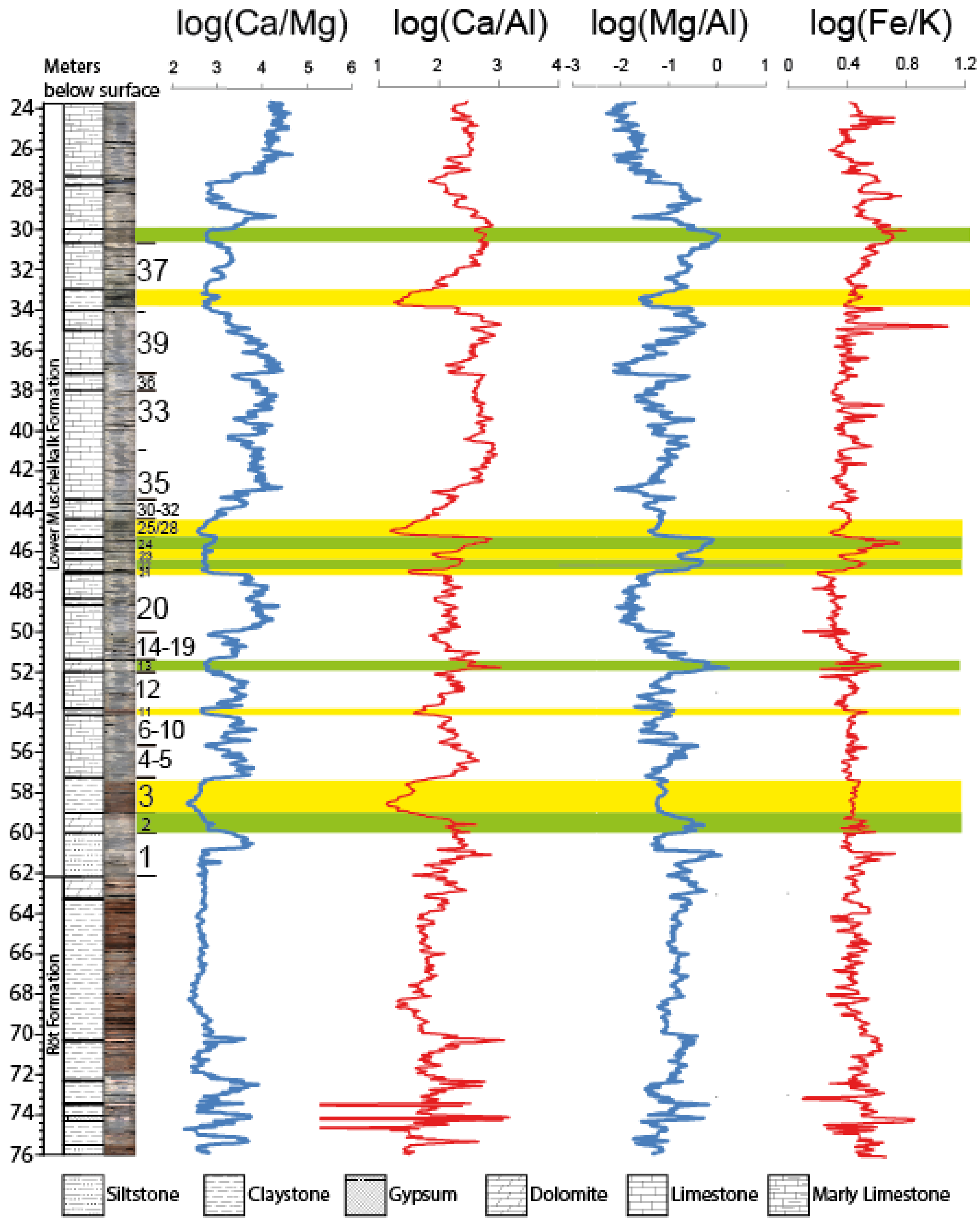

Fig. 5: Similar to Fig. 3, but now with a different set of proxies. Ca/Al is similar over Ca/Ti and Ca/Fe as it reflects terrestrial (lithogenic) vs marine (biogenic) input, and shows negative shifts within the claystone intervals. Ca/Mg was used to determine the position of the dolostones within the LMW. However, Mg is high for both dolostones and claystones. Therefore it was normalised to Al, which only has a high concentration within the claystones, yielding the Mg/Al proxy. This proxy only shows high values for the dolostone intervals and can therefore be used as a dolostone indicator. The correlation between the dolostone intervals and peaks in Mg/Al is indicated by the green bars. The Fe/K proxy was plotted because it may reflect hinterland humidity, although it shows no significant variations throughout the core.

PC	Eigenvalue	% variance
1	6738.5	88.584
2	749.267	9.8498
3	111.41	1.4646
4	5.1007	0.067054
5	1.63331	0.021471
6	0.572847	0.0075306
7	0.351514	0.004621
8	0.0315076	0.0004142
9	0.0097067	0.0001276
10	0.00717972	9.4384E-05
11	0.00441765	5.8074E-05
12	0.00365136	4.8001E-05
13	0.00154299	2.0284E-05
14	0.00072210	9.4927E-06
15	0.00048812	6.4169E-06
16	0.00021327	2.8036E-06

Table 1: Principal components for the analysis of the elements Mg, Al, Si, S, Cl, K, Ca, Ti, Cr, Mn, Fe, Br, Rb, Zr, Pb, Sr and Ba, showing both eigenvalues and variance. Since the first two principal components explain 98.4338 % of the variance seen within the data, the analysis is valid. The first principal component is very strong as it explains 88,584 % of the total variance of the data, while PC2 accounts for 9.8498 % of the total variance. The contribution of the other principal components is very small, as they explain only 2.6 % of the total variance and are therefore excluded from further analysis.

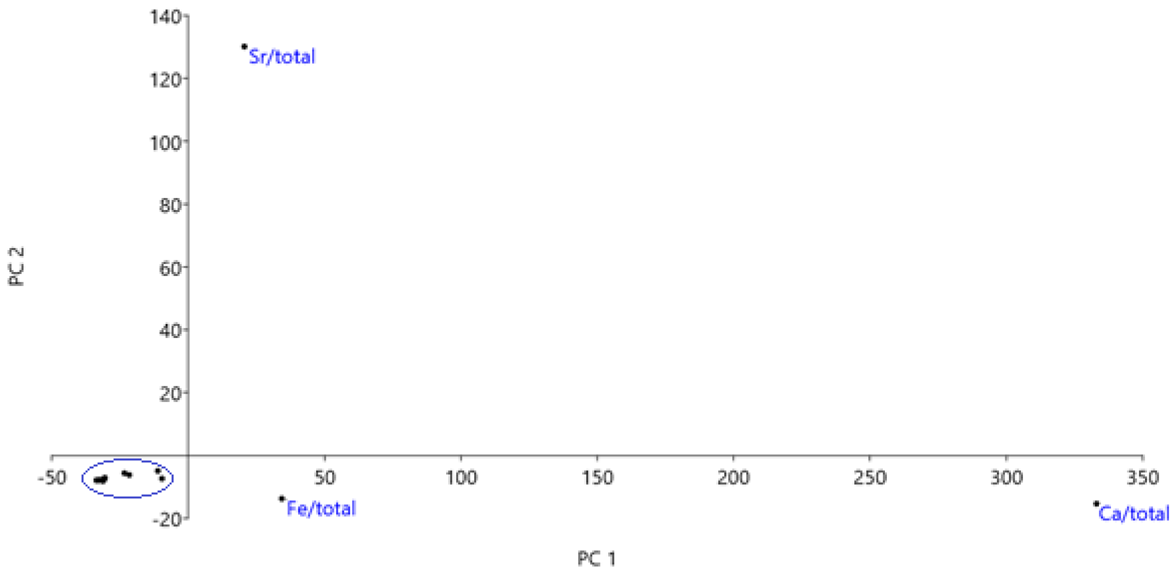

Fig. 6: XY-plot of the first two components that shows the most important geochemical end - members: 1 = Ca/total, 2 = Sr/total, 3 =Fe/total and 4 = the other elements within the blue circle.

	Al/total	Si/total	K/total	Ca/total	Ti/total	Fe/total
Al/total		0	0	0	0	0
Si/total	0.98309		0	0	0	0
K/total	0.97462	0.95693		0	0	0
Ca/total	-0.94561	-0.95078	-0.94016		0	0
Ti/total	0.97261	0.97499	0.95203	-0.97159		0
Fe/total	0.87764	0.86878	0.87514	-0.93332	0.88343	

Table 2: Correlation matrix of Al, Si, K, Ca, Ti and Fe. Values for correlation are given in the lower triangle, with 1 being a 100 % positive correlation and -1 being a 100 % negative correlation. Note that correlation values are independent of the amount of element columns chosen as input, so taking only a few elements from the data set will not alter their mutual correlation values. The two-tailed probabilities that columns may be uncorrelated are displayed in the upper triangle of the matrix, which are all displayed as zero.

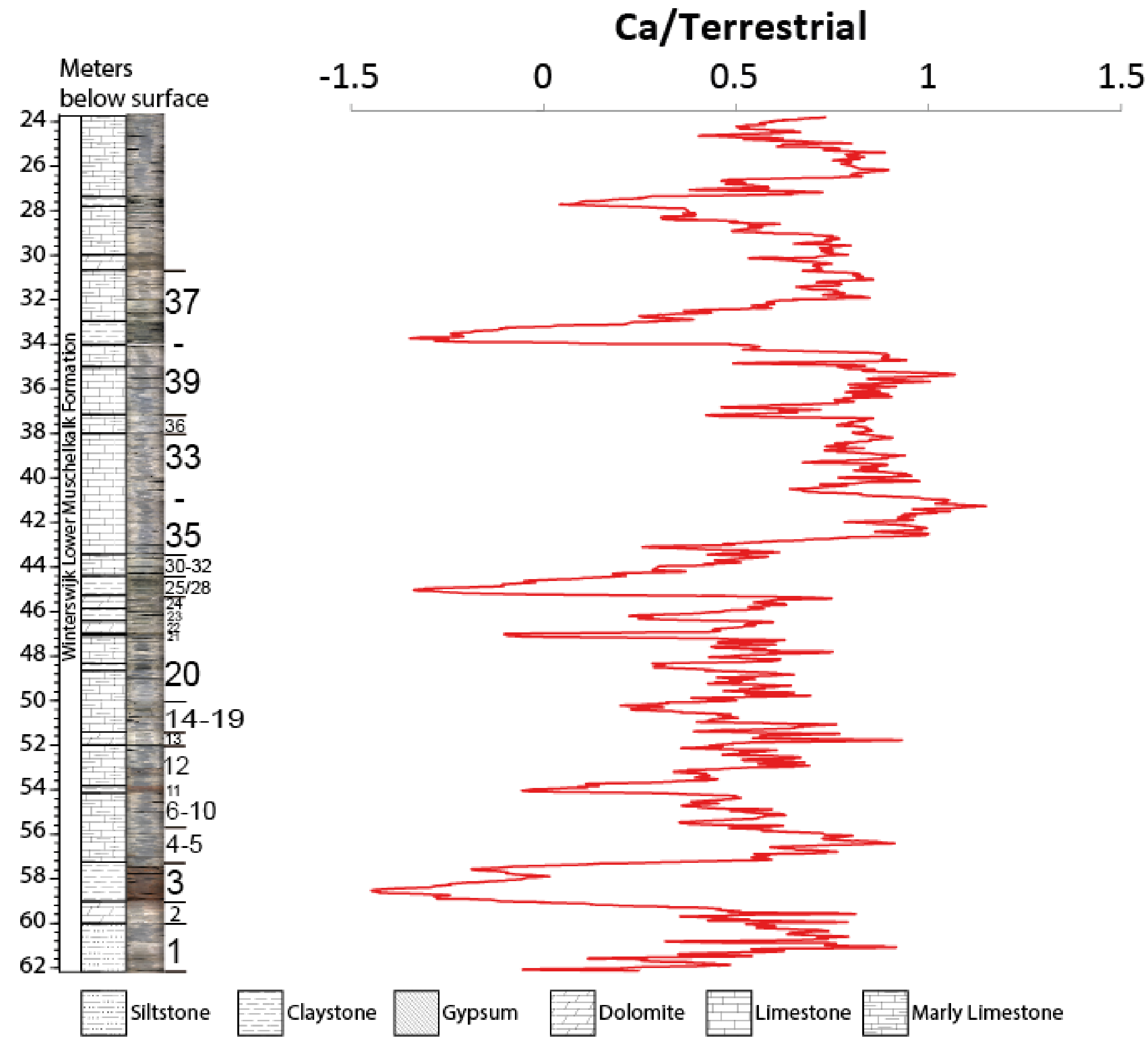

Fig. 7: Plot of the LMW lithology and the Ca/terrestrial ratio in the depth domain. The left two columns represent the lithological and photo log of the LMW respectively with the Oosterink numbers (Oosterink, 1986). The Ca/Terrestrial is the log ratio of Ca/total divided by (Al+Si+Fe+K+Ti)/total. The depth axis is given in meters below surface.

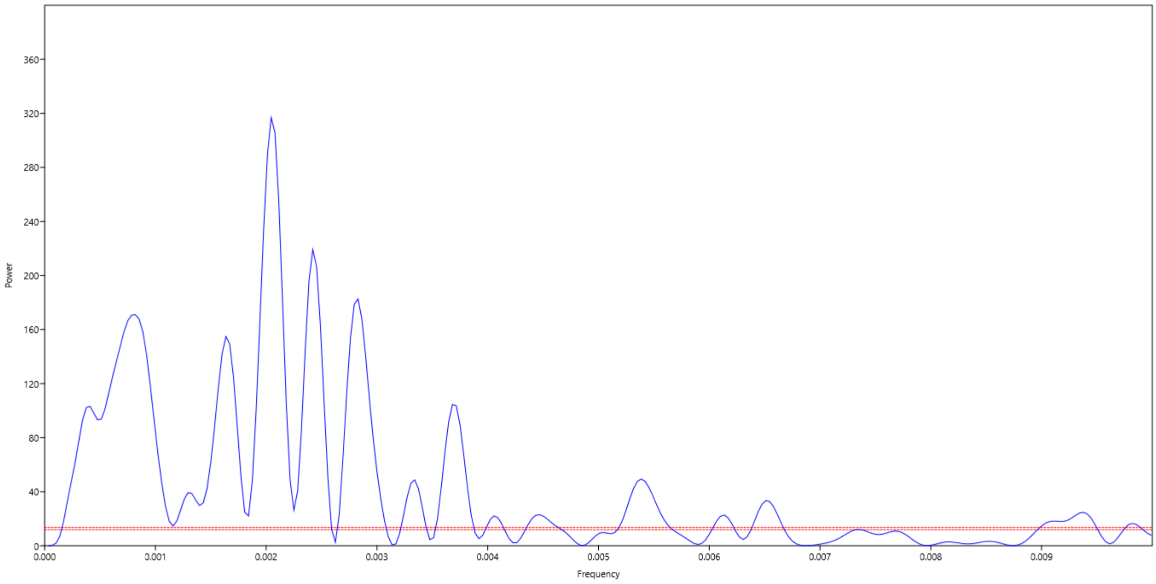

Fig. 8: Lomb periodigram of Ca/Terrestrial for the LMW, with the frequency expressed as 1/cm. The red line indicates the $p < 0.01$ confidence interval. Major peaks occur at frequencies of $8.33*10^{-4}$, $1.62*10^{-3}$, $2.04*10^{-3}$, $2.46*10^{-3}$ and $2.87*10^{-3}$, while smaller peaks are present at frequencies of $3.28*10^{-3}$, $3.66*10^{-3}$, $4.54*10^{-3}$, $5.37*10^{-3}$, $6.08\text{^}10^{-3}$, $6.51*10^{-3}$ and $9.04*10^{-3}$.

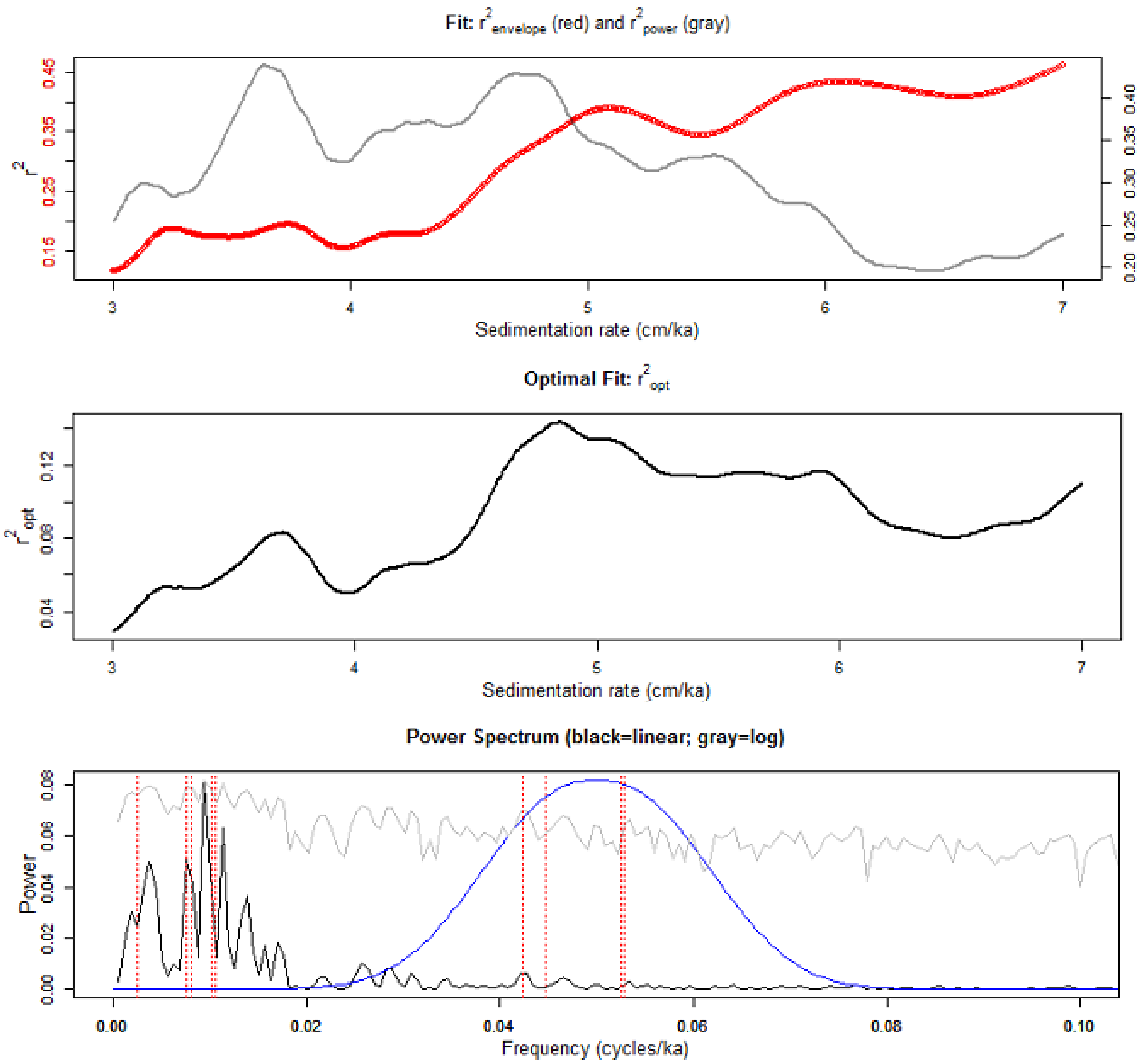

Fig. 9: TimeOpt run with sedimentation rate limits from 3 to 7 cm/kyr. Upper Fig.: fits of the spectral power R^2 power (gray) and the amplitude modulation of precession R^2 envelope (red) for each given sedimentation rate. Middle Fig.: optimal fit as product of the values of R^2power and R^2envelope for each given sedimentation rate. Bottom Fig.: periodigram with the sedimentation rate derived from the peak optimal fit (black line is A linear spectrum; grey line is a log spectrum). Vertical red lines indicate the target orbital periods and the blue line the area of the expected precession modulation.

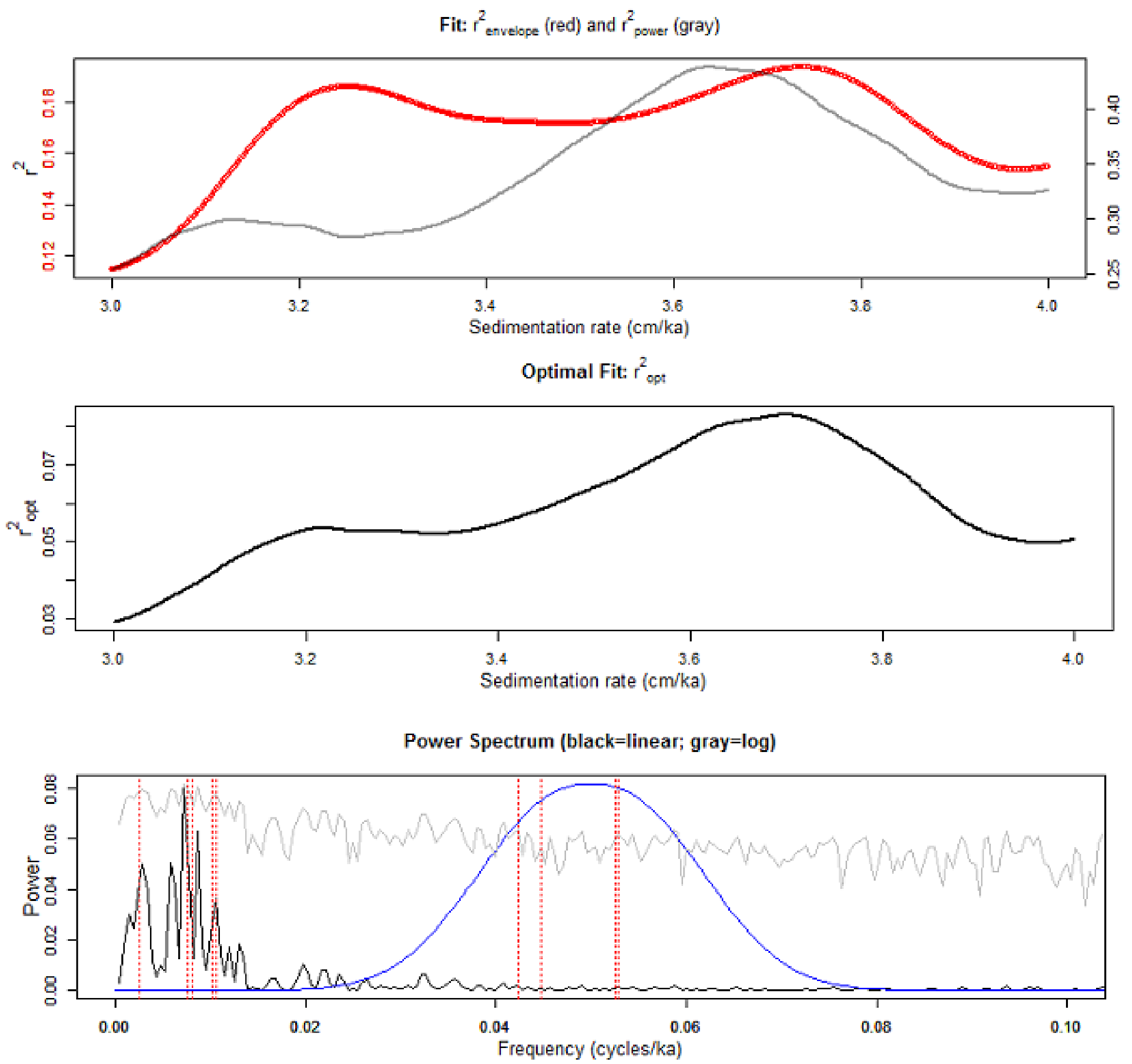

Fig. 10: Similar to Fig. 9 but now with sedimentation rate limits from 3 to 4 cm/kyr

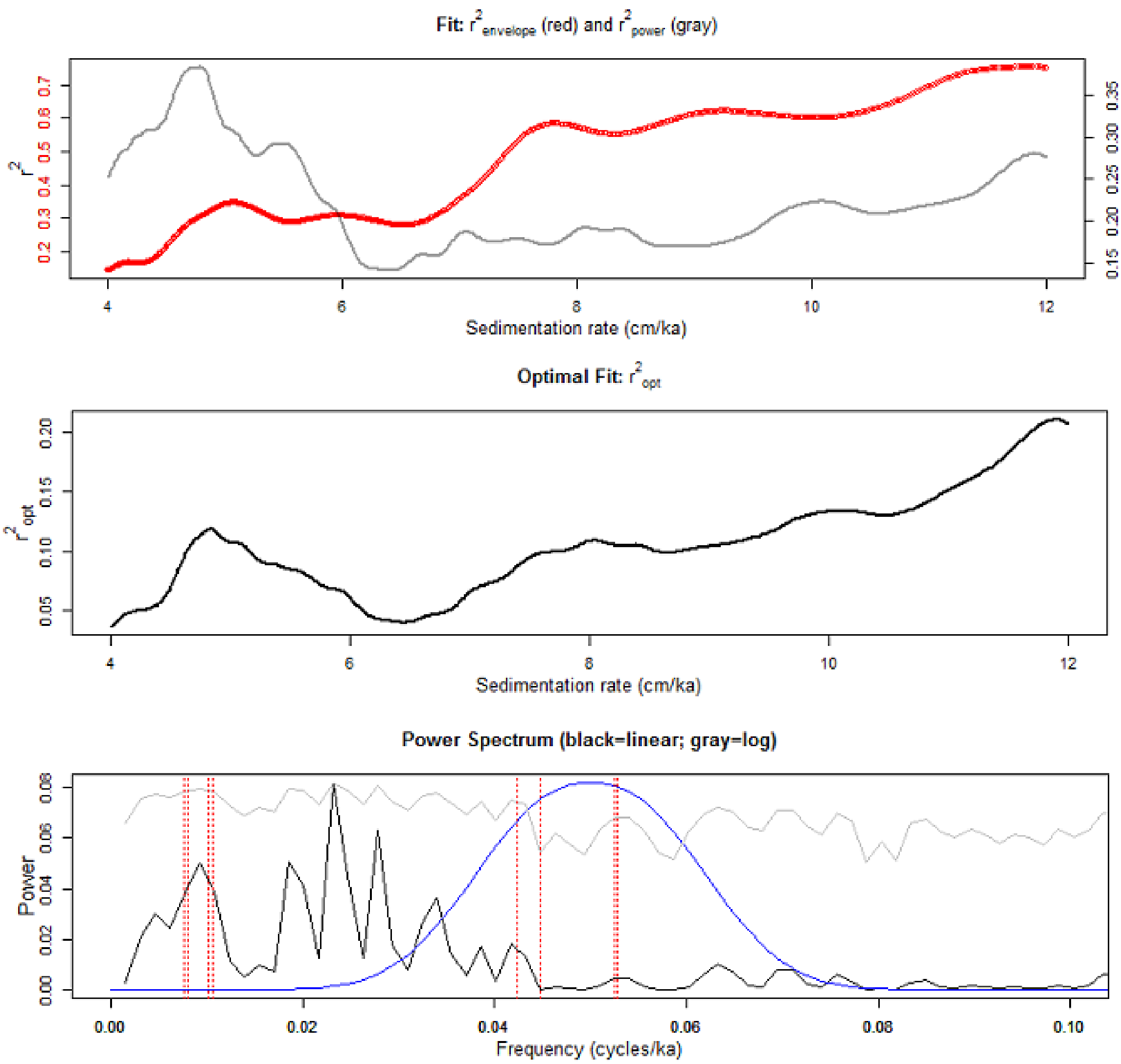

Fig. 11: Same as Fig. 9, but now run with sedimentation rates from 8 -12 cm and without considering the 405 kyr cycle.

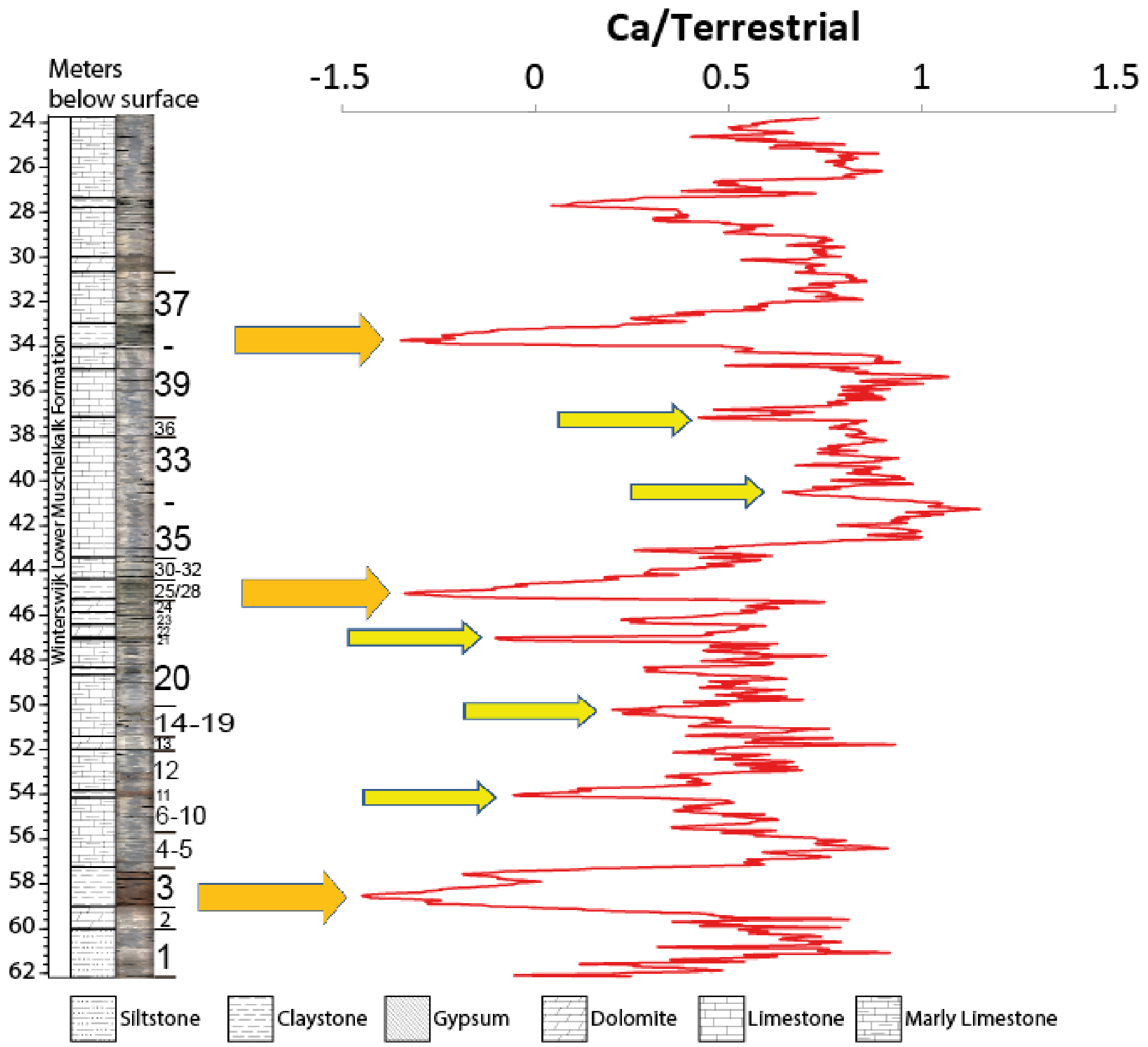

Fig. 12: Ca/Terrestrial proxy with depth in meters below surface (mbs). The orange arrows indicate the peaks of the largest in-depth cycle which has an average period of 12 meter on average, while the yellow arrows show the peaks of the 3.5 – 4.1 meter cycle. The interval above 31 mbs remains unidentified in terms of cyclicity due to change in peak amplitude and period.

Astronomical cycle	Duration	In-depth thickness with 12 meter tuned to the long eccentricity period	In-depth period with 12 meter tuned to the short eccentricity period
Long eccentricity	405.7 kyr	11.5 -13 meter	37.9 – 52. 5 meter Not found/detectable
Short eccentricity	130.7 – 94.9 kyr	3.5 - 4 meter	11.5 -13 meter
Precession	23.6 – 18.9 kyr	0.7 – 0.6 meter Not found/detectable	1.8 - 3.0 meter
Estimated sedimentation rate	-	3.0 cm/kyr	9.3 – 12.9 cm/kyr
TimeOpt derived sedimentation rate	-	3.7 cm/kyr	
Total estimated duration for LMW deposition expected	-	1.3 Myr	360 – 498 kyr
Total duration for LMW deposition based on TimeOpt results	-	1.0 Myr	
Agreement between TimeOpt and expected results	-	Yes	No

Table 3: Astronomical periods with durations and theoretical in-depth thickness for two scenarios: 1) the 12 meter cycle tuned to the long eccentricity period and 2) the 12meter cycle tuned to the short eccentricity period. Estimated sedimentation rates and age durations were based on the fit between the 12 meter cycle and the target astronomical period. Sedimentation rates for peak spectral power in TimeOpt with corresponding age durations.